Appl. Phys. B 91, 177–181 (2008)
DOI: 10.1007/s00340-008-2942-5

Applied Physics B
Lasers and Optics

H. OU[1,✉]
T.P. RØRDAM[1]
K. ROTTWITT[1]
F. GRUMSEN[2]
A. HORSEWELL[2]
R.W. BERG[3]
P. SHI[4]

Ge nanoclusters in PECVD-deposited glass caused only by heat treatment

[1] COM·DTU, Technical University of Denmark (DTU), Building 345v, 2800 Kgs. Lyngby, Denmark
[2] Department of Manufacturing Engineering and Management, Technical University of Denmark (DTU), Building 201, 2800 Kgs. Lyngby, Denmark
[3] Department of Chemistry, Technical University of Denmark (DTU), Building 207, 2800 Kgs. Lyngby, Denmark
[4] Danchip, Technical University of Denmark (DTU), Building 346, 2800 Kgs. Lyngby, Denmark

Received: 16 August 2007/Revised version: 9 January 2008
Published online: 19 February 2008 • **© Springer-Verlag 2008**

ABSTRACT This paper reports the formation of Ge nanoclusters in a multi-layer structure consisting of alternating thin films of Ge-doped silica glass and SiGe, deposited by plasma-enhanced chemical vapor deposition (PECVD) and post annealed at 1100 °C in N_2 atmosphere. We studied the annealed samples by transmission electron microscopy (TEM) and Raman spectroscopy. As-deposited and annealed samples were analyzed by secondary ion mass spectroscopy (SIMS). TEM investigation shows that Ge nanoclusters were formed in the as-deposited SiGe layer and the SiGe layer was transformed into a silicon dioxide layer embedded with Ge nanoclusters after annealing. These nanoclusters are crystalline and varied in size. There were no clusters in the Ge-doped glass layer. Raman spectra verified the existence of crystalline Ge clusters. The positional shift of the Ge vibrational peak with the change of the focus depth indicates that the distribution of the stress applied to the Ge clusters varies with depth. SIMS measurements show clearly the dramatic O increase in the as-deposited SiGe layer after annealing. The creation of Ge nanoclusters by the combination of PECVD and annealing makes possible the application in complicated waveguide components.

PACS 81.07.Bc; 78.66.Jg; 42.65.Wi

1 Introduction

Ge nanoclusters (nc) embedded in silica matrices have attracted intensive research interest during the past decade due to the unique electric and photonic properties, brought about by the quantum-confinement effect, and their potential applications in new-generation devices. Among these, optical memories [1, 2], light emitters [3–8] and enhanced third order optical nonlinearity [9–13] are the three main fields into which much effort has been put. At present, Ge nc have been successfully made by a lot of methods. The film deposition methods have encompassed radio-frequency (rf) or magnetron co-sputtering [3, 5, 6, 9, 11, 13–16], ion implantation [10, 17–20], oxidizing of SiGe [2, 8] and plasma-enhanced chemical vapor deposition (PECVD) [21, 22]. After the deposition, the film is usually post processed by annealing, electron-beam irradiation or both. However, none of the methods can pre-design the size, concentration and distribution of the Ge nc, which stimulates further investigation of this material.

In this study, PECVD was used to deposit films, and annealing was applied to form Ge nc in the silica matrix. One of our earlier papers [22] reported that Ge nc had been made by the combination of PECVD, annealing and electron-beam irradiation. As expected, the electron beam irradiation method can hardly make large amounts of Ge nc in a large area. Therefore, that method cannot be applied for nonlinear planar waveguide components. However, the making of Ge nc only with PECVD and annealing, without subsequent electron-beam irradiation, as reported in this paper, opens up a promising method for fabricating enhanced third order nonlinearity silica waveguide components.

2 Experiments

Multi-layer films were deposited by using PECVD (STS cluster system) with the alternation of Ge-doped glass layers and amorphous SiGe layers. The deposition started with a Ge-doped glass layer on top of a 4-in, (001)-oriented, 525-μm-thick silicon wafer. This deposition used 5 sccm (standard cubic centimeters per minute) SiH_4, 5 sccm GeH_4 and 1600 sccm N_2O as reaction gases, at a temperature of 300 °C, a process pressure of 400 mTorr (∼ 50 Pa) and an applied rf power of 600 W. Then, an amorphous SiGe layer was deposited by switching off the N_2O, while keeping the remaining parameters like 5 sccm SiH_4, 5 sccm GeH_4, pressure and power the same as for glass deposition. The deposition time of the glass was 5 min and the SiGe layer deposition time was set at 1 min, which led to a 0.5-μm-thick glass layer and a 0.14-μm-thick SiGe layer, respectively. A four-layer structure consists of two pairs of glass layer and SiGe layer. The second pair of Ge-doped glass layer and SiGe layer was deposited in sequence on top of the first pair.

After the deposition, the thin films were annealed at 1100 °C for 4 h in dry N_2 at ambient pressure.

✉ Fax: +45-4593-6581, E-mail: ho@com.dtu.dk

The prepared samples were examined by transmission electron microscopy (TEM) using a JEOL JEM-3000F operated at 300 kV.

The Raman spectra were measured at room temperature by using a DILOR XY spectrometer with a liquid nitrogen cooled CCD detector (140 K) and a microscope entrance. All the spectra were excited with the 514.5-nm line from an argon-ion laser. Calibration of the wavenumber scale was done to an accuracy of $\pm 1\ \mathrm{cm}^{-1}$ with liquid cyclohexane and neon gas lines superimposed on the spectra.

Secondary ion mass spectroscopy (SIMS) was performed using an ATOMIKA 4000 with an O_2^+- or Cs^+-ion source. The beam energy ranged between 1 and 15 keV. A quadruple mass analyzer was used.

3 Results and discussion

3.1 *TEM and HRTEM*

As described in an earlier paper [22], irradiation by an electron beam plays an important role during the formation of Ge nanoclusters from Ge-doped glass. Therefore, extreme caution has been taken here to reduce the effect of the electron beam when TEM images were recorded. An image of a four-layer structure after annealing is shown in

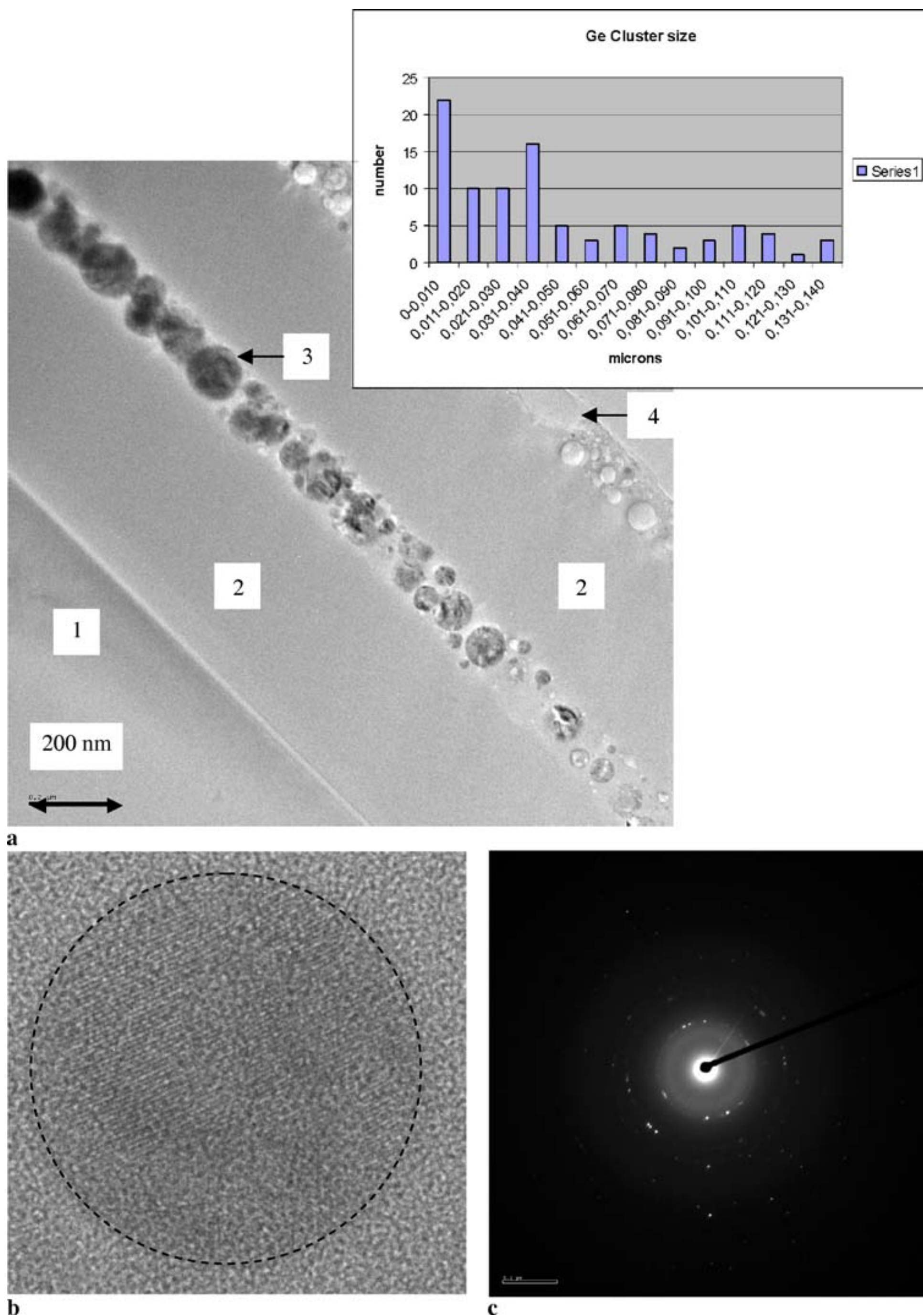

FIGURE 1 (**a**) TEM image of a four-layer structure: Si substrate is indicated as 1; two Ge-doped glass layers are indicated as 2; layer containing embedded Ge nanoclusters is 3 and porous top layer is 4. *Inset* is the size histogram of Ge nanoclusters in layer 3; (**b**) HRTEM image showing crystal planes of one round cluster; (**c**) selected area diffraction patterns confirm excellent crystallinity of the nanoclusters, without including Si substrate

Fig. 1a. One 140-nm-thick layer with dark Ge nanoclusters was clearly seen, marked as number 3 in Fig. 1a. These clusters vary in size, and the maximum diameter of the clusters is 140 nm, which is the thickness of this layer. The inset is the size histogram of these clusters. The number of the clusters decreases exponentially as the diameters of the clusters increase. By tuning the thickness of the SiGe layer, the maximum diameter of the clusters can be tuned at the same time. However, there is an upper limit for the maximum diameter. Under our deposition conditions, a 500-nm-thick SiGe layer broke after annealing. These clusters appear as round and darker dots due to increased mass contrast. The Ge-doped glass layer (SiO_2:Ge) is 500-nm thick, marked as 2 in Fig. 1a. Another 140-nm-thick porous layer is seen on the top surface, marked as 4 in Fig. 1a. The formation of the porous surface layer is due to the evaporation of the Ge clusters during annealing at 1100 °C. In comparison with layer 2, layer 3 (excluding the dark Ge clusters) is much whiter, which implies a much lower Ge concentration in this layer.

A high-resolution transmission electron microscopy (HRTEM) image of one of the clusters is shown in Fig. 1b. Perfect lattice fringes are visible.

A selected area diffraction pattern (SADP) from the clusters is shown in Fig. 1c. A clear diffraction pattern exhibiting sharp spots is present, showing that the clusters are crystalline.

Composition of the different layers was analyzed by energy dispersive X-ray spectroscopy (EDS) during the TEM investigation. It was found that the initial SiGe layer was turned into a SiO_2 layer with embedded Ge nanoclusters after annealing. This was further confirmed by the SIMS measurements in Sect. 3.3.

3.2 *Raman spectroscopy*

Raman spectra of the same sample investigated by the above TEM were recorded from the top surface. Spectra of bulk silicon and germanium specimens were also recorded as references. In Fig. 2a, six curves are shown. Curves Ge and Si are from mono-crystalline bulk reference materials.

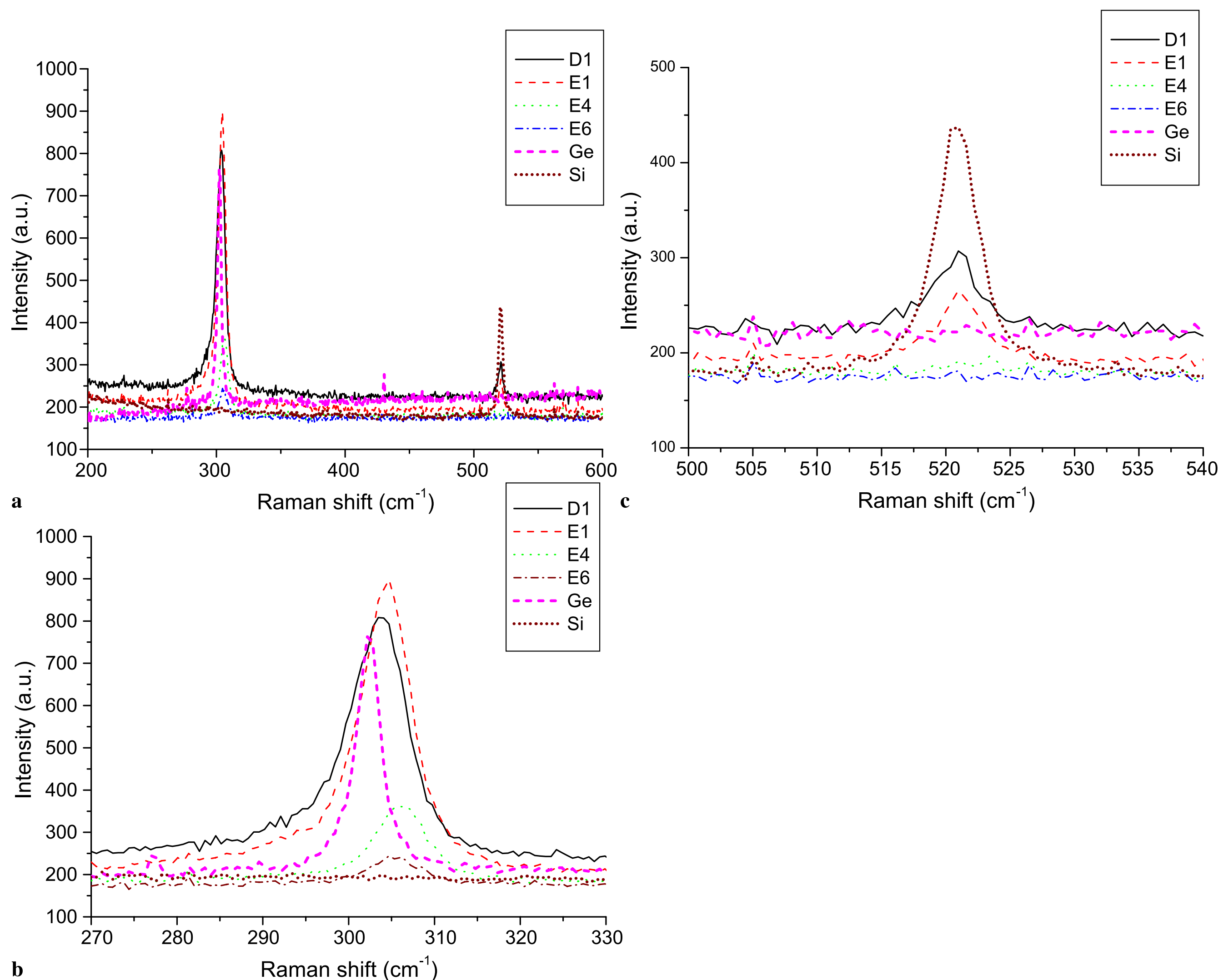

FIGURE 2 (**a**) Raman spectra from sample with Ge nc. Spectra from bulk Si and Ge are included as references. Spectra D1, E1, E4 and E6 were collected when changing the focus from the top surface of the sample to deep inside the substrate; (**b**) expanded view of Ge peak; (**c**) expanded view of Si peak

Curves D1, E1, E4 and E6 are from the same spot on the sample while changing the focus of the microscope from the top surface to deep inside the substrate. These four curves have two prominent peaks; one is located at $\sim 300\,cm^{-1}$, contributed from Ge, and the other is at $520\,cm^{-1}$, contributed from Si. Expanded views of these two peaks are shown in Fig. 2b and c for details. From Fig. 2b, we can see that the intensity of the $300\,cm^{-1}$ peak increases first, reaches a maximum and then decreases as the focus is changed from the top surface to deep inside the substrate. The peak is strongest when the Ge nanocluster layer is in focus. The further the focus is away from the Ge nc layer, the weaker the peak becomes. Compared with the mono-crystalline Ge peak at $302.1\,cm^{-1}$, the peaks from Ge nc shift to $303.6\,cm^{-1}$, $304.8\,cm^{-1}$, $306.2\,cm^{-1}$ and $305.8\,cm^{-1}$ corresponding to curves D1, E1, E4 and E6, respectively. Moreover, the peaks from Ge nc are broader than that from mono-crystalline Ge. According to [16], a probable cause of the shift of the Raman peaks is internal stress, with compressive stress exerted on the clusters causing the shift of the peaks to longer wavelengths. Therefore, we infer that the Ge nc in our structure experience compressive stress and that the magnitude of the stress on these Ge nc at different depths in the layer may have different values. The broadening of the Raman peak may be attributed either to the size distributions in Ge nc [23] or to the size dependence of the stress-induced line shift.

Another point from Fig. 2b is that the Ge nc peak in curves D1 and E1 is even stronger than that in mono-crystalline bulk Ge. The reason could be the quantum effect or a porous top layer acting as a surface enhancement. Further investigations are being carried out to clarify this.

From Fig. 2c, the Si peak is seen to be insensitive to changes in the focus. For all the curves, this peak is located at $520.9\,cm^{-1}$, about the same as bulk Si, and the silicon peak is much weaker than the Ge peak. The position of the peak overlaps with the mono-crystalline bulk Si, which indicates that it comes from the Si substrate. The intensity ratio of the Ge peak to the Si peak is almost the same for different focuses. The absence of a signal at around $400\,cm^{-1}$, which would be related to Si–Ge bonds, further supports the nanoclusters being composed of Ge exclusively.

Another conclusion that can be drawn from the weak Si peak is that Ge nc absorbed strongly at the wavelength of 514.5 nm (Raman pump light) and 528.7 nm (Si Raman shift). Little pump light can pass Ge nc and reach the Si substrate, and even less Raman scattered light from the Si substrate can go through the Ge nc again and be collected by the detector.

3.3 *SIMS*

In order to analyze the composition change, especially in the Ge nanocluster layer, a trilayer structure (a glass layer ending as the top surface layer, acting as a cap to avoid evaporation of Ge during annealing) was prepared and SIMS measurements were made for both as-deposited samples and annealed samples for comparison. Three elements (O, Si and Ge) were analyzed through the three layers and the results are shown in Fig. 3a and b, respectively. Three interfaces (SiO_2–Ge nc, Ge nc–SiO_2 and SiO_2–Si) are clearly observed in both figures. Comparing Fig. 3a and b, there is no visible difference for the Ge-doped glass layer. They have almost the same concentration with respect to elements O, Si and Ge. However, a big difference is seen in the middle SiGe layer. After annealing, O composition in the middle layer increases dramatically. Since the sample was annealed in N_2 at ambient pressure, the increase of O must come from the surrounding Ge-doped glass layer. The O source from the glass layer could be some content of O-rich non-stoichiometric SiO_2:Ge. The O could be released and diffused to the middle SiGe layer during the annealing, and turned the as-deposited SiGe layer into a SiO_2 layer with Ge nc. The possibility of oxygen coming as residual amounts from annealing gas was eliminated here after an experiment. In this experiment, the same annealing recipe was used to anneal Si wafers. The oxide thicknesses before and after the annealing were measured to be 1.2 nm and 2.3 nm, respectively. The thickness increase of the oxide was assigned to oxidization during the loading and unloading of wafers at 700 °C for about 10 min.

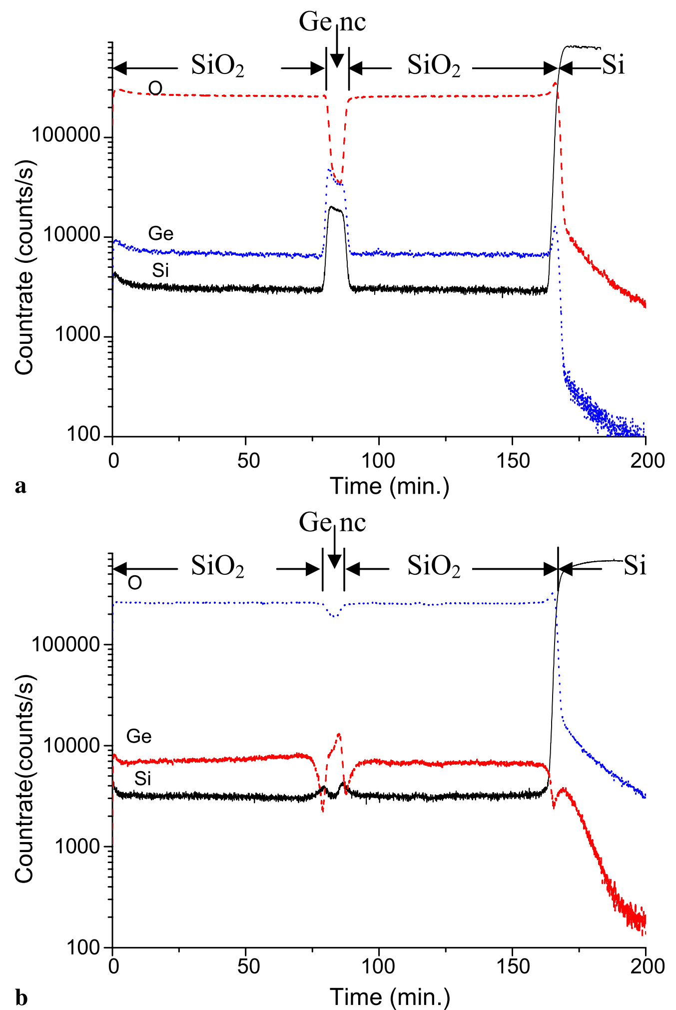

FIGURE 3 (**a**) SIMS depth profile of the as-deposited trilayer structure on top of Si substrate. *Solid black line*, *dotted blue line* and *dashed red line* are secondary ion intensities of Si, Ge and O, respectively; (**b**) SIMS depth profile of the trilayer structure after annealing at 1100 °C for 4 h. *Solid black line*, *dotted blue line* and *dashed red line* are the secondary ion intensities of Si, O and Ge, respectively

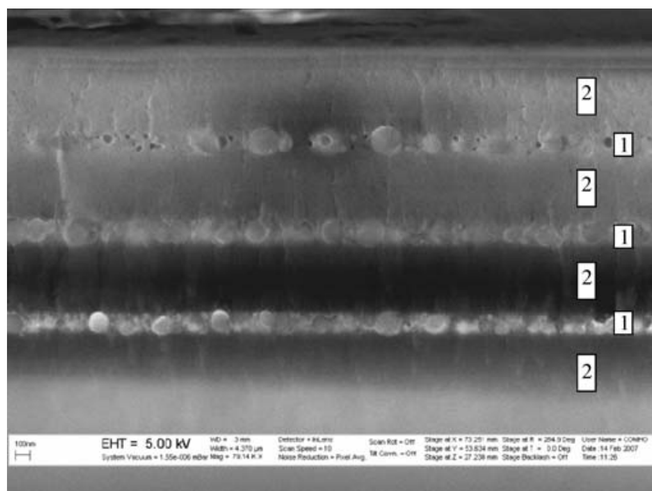

FIGURE 4 SEM image of a seven-layer structure: three Ge nc stripes (marked as 1) plus four glass layers (marked as 2)

3.4 *Multi-Ge nanocluster-layer structure*

Multi-Ge nc-layer structures can readily be achieved by using the described PECVD deposition followed by annealing. To illustrate this, a scanning electron microscope (SEM) image of a seven-layer structure is shown in Fig. 4, where three Ge nc layers were sandwiched by four glass layers. Since one of the potential applications of this structure is the fabrication of nonlinear waveguide components, this method can be easily adopted for mass production.

4 Conclusion

Ge nc were successfully synthesized in a SiO_2 matrix by the combination of PECVD and post annealing. A four-layer structure with alternating glass layers and SiGe layers was deposited by PECVD. After annealing at 1100 °C in N_2 for 4 h, the SiGe layers were turned into glass layers with embedded Ge nanoclusters. The Ge nc varied in size. The maximum diameter was 150 nm. HRTEM and electron diffraction verified that all the clusters were made of Ge, and were crystalline without noticeable defects. Raman spectra confirmed the presence of crystalline Ge nc. The strong Ge peak shifted to longer wavelengths compared to bulk mono-crystalline Ge. Furthermore, the Ge peak from the same spot on the sample shifted as the focus was changed from the top surface of the chip to deep inside the substrate. This shift is interpreted to indicate the difference of the stress the Ge nc experience with depth. SIMS analysis confirmed that an as-deposited SiGe layer was turned into a glass matrix embedded with Ge nc. The oxygen source for this modification was discussed and probably is from the O-rich non-stoichiometric SiO_2:Ge. A seven-layer structure was fabricated by the same method and was shown to be a good candidate to make complicated waveguide components.

ACKNOWLEDGEMENTS The Danish Technical Research Council is thanked for financial support.

REFERENCES

1 C.L. Heng, Y.J. Liu, A.T.S. Wee, T.G. Finstad, J. Cryst. Growth **262**, 95 (2004)
2 J.H. Wu, P.W. Li, Semicond. Sci. Technol. **22**, 89 (2007)
3 T.V. Torchynska, J. Aguilar-Hernandex, L. Schacht Hernandez, G. Polupan, Y. Goldstein, A. Many, J. Jedrzejewski, A. Kolobov, Microelectron. Eng. **66**, 83 (2003)
4 A.K. Dutta, Appl. Phys. Lett. **68**, 1189 (1996)
5 Y. Maeda, N. Tsukamoto, Y. Yazawa, Appl. Phys. Lett. **59**, 3168 (1991)
6 W.K. Choi, Y.W. Ho, S.P. Ng, V. Ng, J. Appl. Phys. **89**, 2168 (2001)
7 H. Yang, X. Yao, S. Xie, X. Wang, S. Liu, Y. Fang, X. Gu, F. Wang, Opt. Mater. **27**, 725 (2005)
8 A. Rodriguez, M.I. Ortiz, J. Sangrador, T. Rodriguez, M. Avella, A.C. Prieto, A. Torres, J. Jimenez, A. Kling, C. Ballesteros, Nanotechnology **18**, 065702 (2007)
9 Y. Maeda, Phys. Rev. B **51**, 1658 (1995)
10 A. Dowd, R.G. Elliman, M. Samoc, B. Luther-Davies, Appl. Phys. Lett. **74**, 239 (1999)
11 H.P. Li, C.H. Kam, Y.L. Lam, Y.X. Jie, W. Ji, A.T.S. Wee, C.H.A. Huan, Appl. Phys. B **72**, 611 (2001)
12 L.P. Yue, Y.Z. He, J. Mater. Sci. Lett. **15**, 263 (1996)
13 Y.X. Jie, Y.N. Xiong, A.T.S. Wee, C.H.A. Huan, W. Ji, Appl. Phys. Lett. **77**, 3926 (2000)
14 A.V. Kolobov, S.Q. Wei, W.S. Yan, H. Oyanagi, Y. Maeda, K. Tanaka, Phys. Rev. B **67**, 195314 (2003)
15 J. Skov Jensen, T.P. Leervad Pedersen, J. Chevallier, B. Bech Nielsen, A. Nylandsted Larsen, Nanotechnology **17**, 2621 (2006)
16 H.G. Chew, F. Zheng, W.K. Choi, W.K. Chim, Y.L. Foo, E.A. Fitzgerald, Nanotechnology **18**, 065302 (2007)
17 J. Von Borany, R. Grötzschel, K.H. Heinig, A. Markwitz, W. Matz, B. Schmidt, W. Skorupa, Appl. Phys. Lett. **71**, 3215 (1997)
18 K.H. Heinig, B. Schmidt, A. Markwitz, R. Grötzschel, M. Strobel, S. Oswald, Nucl. Instrum. Methods Phys. Res. B **148**, 969 (1999)
19 A. Markwitz, B. Schmidt, W. Matz, R. Grötzschel, A. Mücklich, Nucl. Instrum. Methods Phys. Res. B **142**, 338 (1998)
20 J.M.J. Lopes, F.C. Zawislak, M. Behar, P.F.P. Fichtner, L. Rebohle, W. Skorupa, J. Appl. Phys. **94**, 6059 (2003)
21 S. Agan, A. Dana, A. Aydinli, J. Phys.: Condens. Matter **18**, 5037 (2006)
22 H. Ou, T.P. Rørdam, K. Rottwitt, F. Grumsen, A. Horsewell, R.W. Berg, Appl. Phys. B **87**, 327 (2007)
23 M. Fujii, S. Hayashi, K. Yamamoto, Japan. J. Appl. Phys. **30**, 687 (1991)